

Article

Acoustic Analysis of a Hybrid Propulsion System for Drone Applications

Mădălin Dombrowschi ^{1,2}, Marius Deaconu ¹, Laurentiu Cristea ¹, Tiberius Florian Frigioescu ^{1,2}, Grigore Cican ^{1,2,*}, Gabriel-Petre Badea ^{1,2,*} and Andrei-George Totu ¹

¹ National Research and Development Institute for Gas Turbines—COMOTI, 220D Iuliu Maniu, 061126 Bucharest, Romania; madalin.dombrowschi@comoti.ro (M.D.); marius.deaconu@comoti.ro (M.D.); laurentiu.cristea@comoti.ro (L.C.); tiberius.frigioescu@comoti.ro (T.F.F.); andrei.totu@comoti.ro (A.-G.T.)

² Faculty of Aerospace Engineering, National University of Science and Technology Politehnica Bucharest, 1-7 Polizu Street, 1, 011061 Bucharest, Romania

* Correspondence: grigore.cican@comoti.ro (G.C.); gabriel.badea@comoti.ro (G.-P.B.)

Abstract: This paper aims to conduct an acoustic analysis through noise measurements of a hybrid propulsion system intended for implementation on a drone, from which the main noise sources can be identified for further research on noise reduction techniques. Additionally, the noise was characterized by performing spectral analysis and identifying the tonal components that contribute to the overall noise. The propelling force system consists of a micro-turboshaft coupled with a gearbox connected to an electric generator. The propulsion system consists of a micro-turboshaft coupled with a gearbox connected to an electric generator. The electric current produced by the generator powers an electric ducted fan (EDF). The engine-turbo-engine was tested in free-field conditions for noise generation at different speeds, and for this, an array of microphones was installed, positioned polarly around the system and near the intake and exhaust. Consequently, based on the test results, the acoustic directivity was plotted, revealing that the highest noise levels are at the front and rear of the engine. The noise level at a distance of 1.5 m from the turboengine exceeds 90 dBA at all tested speeds. Spectral analyses of both the far-field acoustic signals (measured with a polar microphone array) and the near-field signals (microphones positioned near the intake and exhaust) revealed that the primary contributors to the overall noise are the micromotor's compressor, specifically the gas dynamic phenomena in the fan (BPF and $2 \times$ BPF). Thus, it was determined that at the intake level, the main noise contribution comes from the high-frequency components of the compressor, while at the exhaust level, the noise mainly originates from the combustion chamber, characterized by low-frequency components (up to 2 kHz). The findings from this study have practical applications in the design and development of quieter drone propulsion systems. By identifying and targeting the primary noise sources, engineers can implement effective noise reduction strategies, leading to drones that are less disruptive in urban environments and other noise-sensitive areas. This can enhance the acceptance and deployment of drone technology in various sectors, including logistics, surveillance, and environmental monitoring.

Keywords: acoustic; directivity; turbo shaft; generator; UAV; measurement



Citation: Dombrowschi, M.; Deaconu, M.; Cristea, L.; Frigioescu, T.F.; Cican, G.; Badea, G.-P.; Totu, A.-G. Acoustic Analysis of a Hybrid Propulsion System for Drone Applications. *Acoustics* **2024**, *6*, 698–712. <https://doi.org/10.3390/acoustics6030038>

Academic Editors: Wiesław Fiebig, Guoyong Jin and Jian Kang

Received: 21 June 2024

Revised: 12 July 2024

Accepted: 22 July 2024

Published: 25 July 2024



Copyright: © 2024 by the authors. Licensee MDPI, Basel, Switzerland. This article is an open access article distributed under the terms and conditions of the Creative Commons Attribution (CC BY) license (<https://creativecommons.org/licenses/by/4.0/>).

1. Introduction

Interest in unmanned aerial vehicles (UAVs) has significantly increased thanks to technological progress, as UAVs can now perform complex and hazardous tasks that are challenging for manned aerial vehicles. Their ease of use, enhanced safety, cost-effectiveness, and reduced environmental impact make UAVs suitable for a variety of long-duration missions in both military and civilian fields. These attributes have positioned UAVs as a vital and rapidly expanding sector in the aerial vehicle market [1,2]. Consequently, drones and UAVs are now integral to many fields, undertaking essential missions for society [3].

UAVs are generally composed of several key components: a flight structure, a propulsion system, an onboard electrical system, a mission-specific payload, a control system, and a communication system. Among these, the propulsion system is particularly critical, as it provides the necessary power for the UAV and plays a pivotal role in mission success. UAV propulsion systems typically include energy sources and power units, which can be either conventional engines or electric engines [4,5].

In terms of energy sources, UAV propulsion systems can be divided into three types: fuel-based, hybrid (combining fuel and electricity), and fully electric systems. Electric propulsion for UAVs can utilize various energy sources, such as lithium batteries, fuel cells, supercapacitors, and solar power. It is well known that electric propulsion systems in UAVs often use high-energy-density permanent magnet engines as their power output devices [6].

One major challenge for electric engine-powered UAVs is their limited range. To address this, several methods are being explored to extend their operational range, including the use of fuel-based thermal propulsion systems or hybrid systems that combine electric power with fossil fuel-based propulsion [7].

Fossil fuel propulsion systems can be categorized into two main types: piston engines and turbine engines. These propulsion types offer benefits such as high payload capacity, extended range, and quick refueling capabilities [8].

UAVs with piston engines typically include a fuel supply system, an engine, a mechanical transmission, and a propeller. The engine serves as the energy converter and power source. Due to propeller limitations, most piston engines are suited for low-speed, low-altitude UAVs [9].

For UAVs requiring higher speed and altitude, turbine engines are more appropriate, making them the preferred power units for UAV propulsion systems [10]. However, both piston and turbine engines have the drawback of generating higher noise levels compared to electric engines.

Purely electric propulsion systems face the primary limitation of battery energy density. Hybrid propulsion systems, which combine electric propulsion with internal combustion engines, offer a solution by providing fuel consumption savings over purely combustion-engine systems. Hybrid propulsion systems for UAVs can be classified into parallel, series, series-parallel, and complex configurations, based on whether the engine directly provides thrust [11].

Sources [12,13] describe parallel and series hybrid systems briefly. In a parallel hybrid setup, the engine and electric engine generator jointly drive the propeller through a mechanical transmission. The electric engine generator ensures the engine operates optimally. Excess engine power is converted to electrical energy by the generator and stored, while insufficient engine power is supplemented by stored electrical energy. In a series hybrid system, the engine drives a generator to produce electrical energy, which then powers an electric engine to rotate the propellers. During flight, the electric engine drives the propeller for thrust during takeoff and landing, while a gas turbine generates electrical energy during high-altitude cruising to extend range.

The series-parallel hybrid configuration combines elements of both series and parallel setups, with the power unit consisting of an engine and an electric engine. Hybrid-propelled drones face the challenge of noise generation. While electric-propelled drones are relatively quiet, producing noise mainly from propellers and engines, hybrid systems also generate noise from piston or turbine engines [14,15].

The noise produced by drones is significant for both human perception and certain detection missions. Minimizing drone noise is essential for specific operations to avoid detection by acoustic methods [16,17].

Current aircraft noise levels, including drones and airplanes, are discussed in [18]. This source shows that the A-weighted maximum noise level at 400 ft for small to medium-sized UAVs ranges from 50.1 to 64.1 dBA. The vehicles measured include the Skywalker X-8, DJI M200, Yuneec Typhoon, and GD28X, with noise levels recorded during a fast, level flyover.

According to the Aircraft Noise and Performance (ANP) database [19,20], the average LA, max at 400 ft for a conventional Airbus A320 (CFM56-5A1 engine) and a Boeing 737-8MAX (CFM Leap1B-27 engine) is 95.6 dB(A) and 90.1 dB(A), respectively.

Source [18] also compares two civil aircraft with two UAVs, noting that small to medium UAVs emit significant high-frequency noise. Conventional fixed-wing aircraft experience high-frequency noise attenuation due to atmospheric absorption over long distances. As highlighted in [21], a critical difference between UAV and conventional aircraft noise is the concentration of acoustic energy in high frequencies. UAVs produce primarily tonal noise with multiple complex tones at the harmonics of each rotor's blade passage frequency (BPF) [22–24].

Since hybrid propulsion in drones involves acoustic elements specific to both electrically powered UAVs and aircraft equipped with turboengines, this paper aims to conduct an acoustic analysis of a system composed of a microturbine engine coupled with a generator to produce electric current that drives an EDF (electric ducted fan)-type consumer. The entire assembly is designed to be installed on drones to enhance flight autonomy for drones powered by EDF systems.

2. Materials and Methods

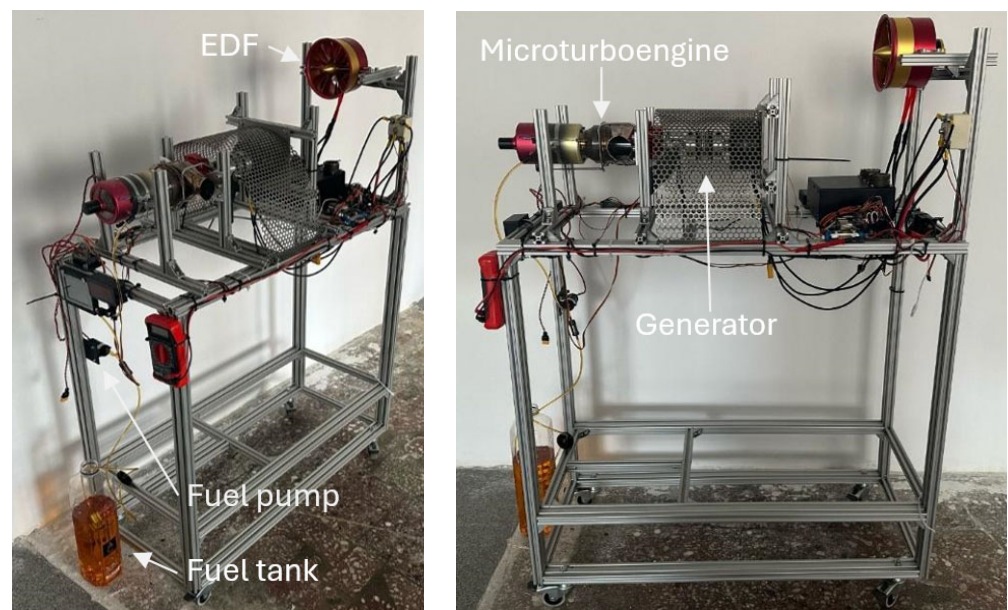
The tests from the present study were performed in a free field and under normal atmospheric conditions, so the sound could propagate freely without any reflections, diffractions, or other interferences from surfaces or objects. This idealized condition allows for the accurate measurement of sound characteristics and the behavior of sound sources without the influences introduced by echoes or reverberations. For these tests, the stand was placed in a free, large area, on grassy land, and far from buildings, ensuring that reflections do not interfere with the direct sound waves. The acoustic measurements were performed using the multi-channel acquisition system DEWESoft SIRIUS® (company Dewesoft d.o.o., Trbovlje, Slovenia) DualCoreADC®, which employs double 24-bit ADCs for each channel, enabling a 160 dB dynamic range across time and frequency domains and a 130 dB signal-to-noise ratio with sample rates up to 200 kS/s per channel and integrated anti-aliasing filtering. The data acquisition system offers over 70 kHz alias-free bandwidth measurements. The acoustic sound pressure signal was recorded with 10 pcs. ½" 40AE microphones (mounted on a GRAS ½-inch Pre-amplifier Type 26CA, which has a frequency range between 2 Hz and 200 kHz) manufactured by G.R.A.S. (Holte, Denmark). This high-precision condenser microphone, designed in compliance with IEC 61094-4 standards, is engineered for accurate sound measurement in free-field environments and is able to measure sound pressure levels ranging from 3.15 Hz to 20 kHz, reaching up to 148 dB. The entire measurement line was calibrated using a Sound Calibrator Type 42AB, manufactured by G.R.A.S., which generates 114 dB (re. 20 µPa) ± 0.2 dB at 1 kHz, IEC 942 (1988) Class 1.

The turbogenerator and the entire system, as shown in Figure 1a, are designed to replicate the operating conditions on a UAV. The system was controlled using a system with two throttles: one for the microengine's fuel flow and another for power, as shown in Figure 1b.

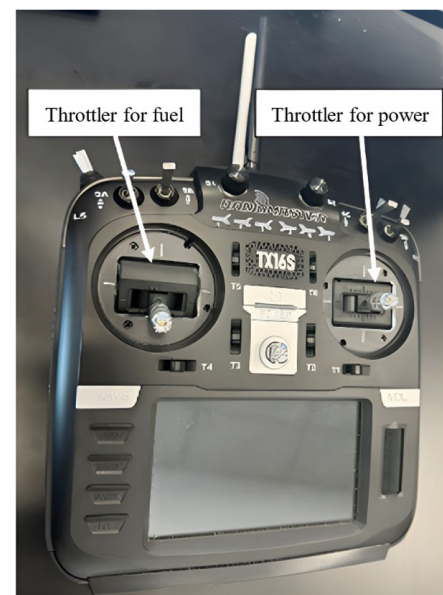
Regarding the acoustic measurements, the entire test setup with microphones arranged around it is shown in Figure 2.

Eight microphones were evenly distributed in a semicircle from the intake axis to the rear of the test stand, at a distance of 1.5 m from the center of the microengine, all positioned at the central axis level of the microengine. The microphone placed at the 0-degree position is microphone M1, and the one placed at the 180-degree position is microphone M8. Two additional microphones were placed near the intake and exhaust at a distance of approximately 300 mm. During the testing campaign, the ambient air temperature was 6.5 degrees Celsius, the humidity was 70%, and the atmospheric pressure was 1008.5 mbar.

Throughout the acoustic measurement campaign, the microengine, part of the turbogenerator unit, was operated across a range of speeds, from idle to a safe upper speed below the maximum. The tests were conducted at an idle speed of approximately 56,000 RPM, then at 75,000 RPM, 90,000 RPM, 103,000 RPM, 115,200 RPM, 123,600 RPM, and 131,640 RPM. These speeds were determined by the load on the consumer. During the tests, the generator's voltage was consistently maintained at 48 V, corresponding to a generator speed of 2800 RPM. The consumer's load was increased from 0 to approximately 1700 W, and at each load increment, the engine was stabilized for about 30 s to record acoustic data. Functional parameters of the stand, such as the voltage and current produced by the generator, were also recorded during the tests to determine the generator's output power.



(a)



(b)

Figure 1. The testing bench configuration (a) and the throttler controller (b).

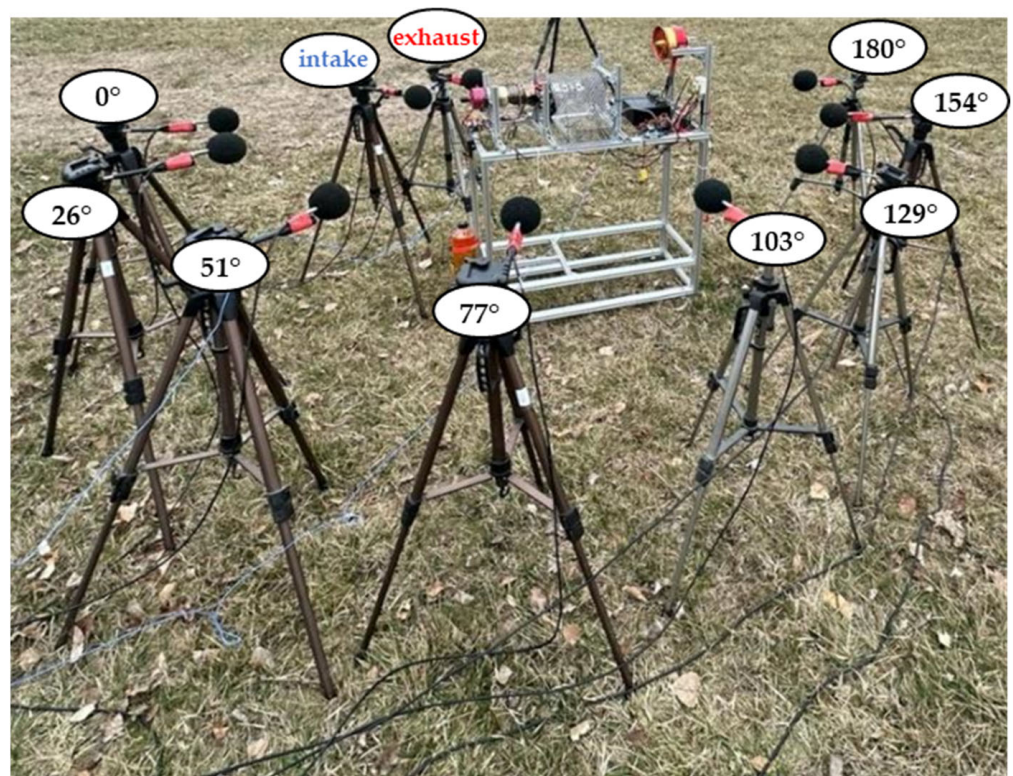


Figure 2. The test bench with microphones arranged around it.

3. Results and Discussions

Following the completion of the experiments, Table 1 presents the acoustic pressure level for each microphone used in correspondence to the rotational speed of the turbo-compressor group of the microengine. The acquisition rate of the recording device was set to 50 kHz, allowing a frequency analysis up to 20 kHz. The overall noise values were computed in the frequency domain from 16 to 20,000 Hz.

Table 1. The acoustic pressure level for each microphone used.

| Microphone | Speed [RPM] | | | | | | |
|------------|------------------------------|--------|--------|---------|---------|---------|---------|
| | 56,000 | 75,000 | 90,000 | 103,000 | 115,200 | 123,600 | 131,640 |
| | Electric Power–Generator [W] | | | | | | |
| | 93.2 | 715 | 1020 | 1245 | 1325 | 1660 | 1707 |
| | Sound Pressure Level [dB] | | | | | | |
| M1 | 97 | 101 | 107 | 102 | 104 | 105 | 107 |
| M2 | 112 | 113 | 113 | 105 | 107 | 107 | 108 |
| M3 | 106 | 106 | 104 | 102 | 103 | 103 | 105 |
| M4 | 104 | 99 | 102 | 102 | 105 | 105 | 107 |
| M5 | 92 | 93 | 97 | 97 | 99 | 102 | 102 |
| M6 | 92 | 95 | 98 | 99 | 100 | 103 | 104 |
| M7 | 91 | 95 | 98 | 101 | 103 | 102 | 106 |
| M8 | 91 | 101 | 104 | 106 | 109 | 109 | 110 |

Based on these values, graphs with the directivity were made on the microengine-electric generator and fan assembly. Thus, Figure 3 shows the acoustic directivity depending on the speed of the microengine.

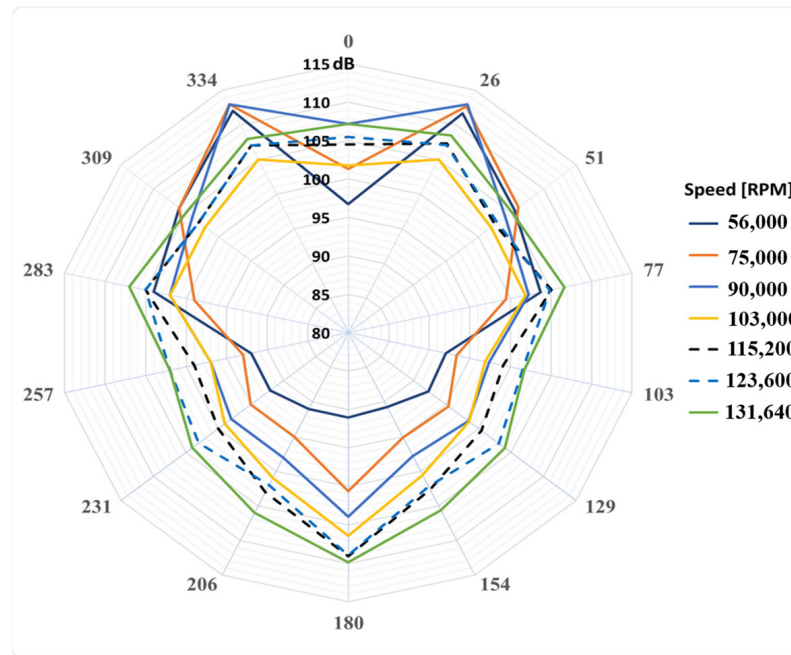


Figure 3. Sound directivity pattern depending on the microengine speed.

From the directivity plot presented in Figure 3, the engine noise radiation is graphically represented. As highlighted in a previous paragraph, at low speeds, the noise is mainly radiated through the engine intake, while the noise from the backside of the test bench has low amplitudes. As the speed increases, the noise directivity tends to become uniform. At an idle speed of 56.000 RPM, at the microphone located at the back of the stand, the global acoustic pressure level is visibly lower than in the other operating modes because, in this mode, the EDF does not start but will enter into function at the next regime. Next, in Figure 4, the overall noise values in the frequency domain of 16–20,000 Hz for all microphones and for all engine regimes are presented.

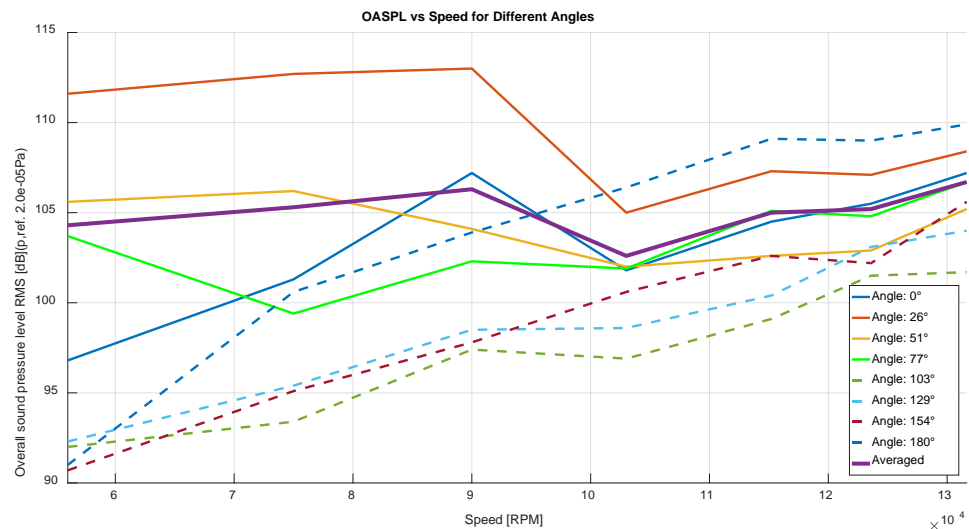


Figure 4. Acoustic pressure level variation for each microphone depending on the speed.

This graph shows the analysis of the noise variation at each measurement point, depending on the speed. The main observation is that there are certain speeds at which the noise decreases; however, with the increase in speed, a general trend of increasing noise of 10 dB is observed for microphones placed from 103° to 180°.

On the other hand, overall noise values measured in microphones from 0 to 77° present a distinct character. Up to 103,000 RPM, the overall noise levels are higher than at other revolutions. Beyond this speed, the noise curves follow the trend of those from the other microphones. To explain this phenomenon, the spectral analysis of each acoustic signal was computed. To better understand the acoustic phenomena presented in Figures 5–12, a detailed analysis of the noise at the level of the microphone at all speeds was carried out. In each figure, the value in degrees for each microphone is shown at the top.

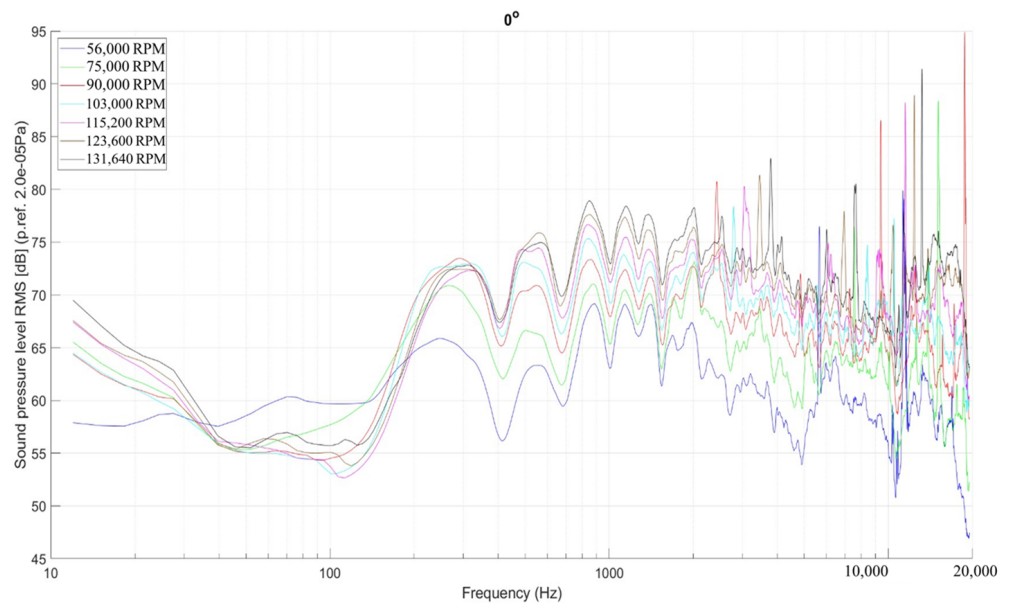


Figure 5. Comparative noise spectral analysis for the M1 microphone (0°) as a function of speed.

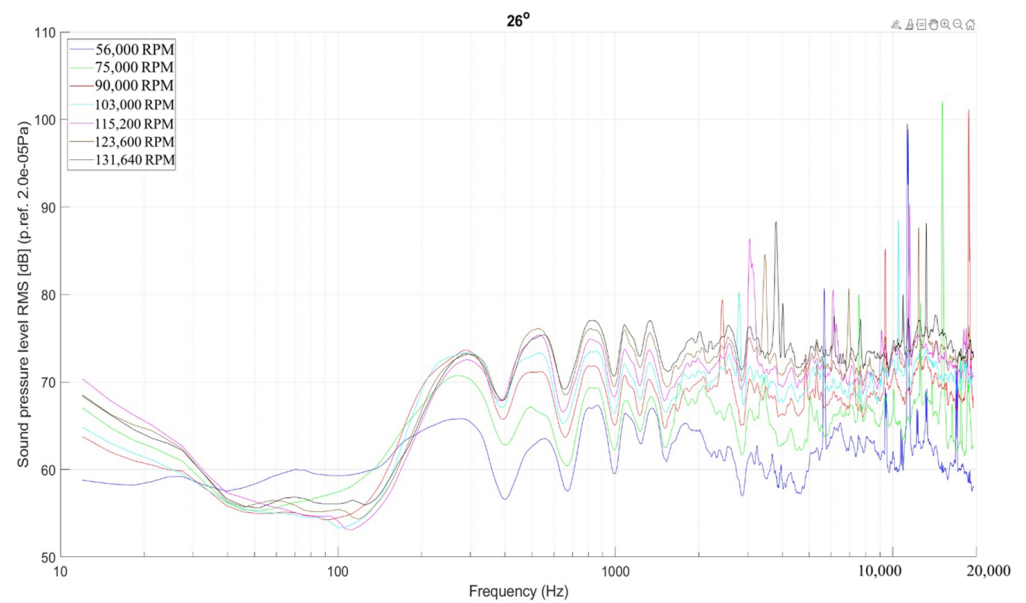


Figure 6. Comparative noise spectral analysis for the M2 microphone (26°) as a function of speed.

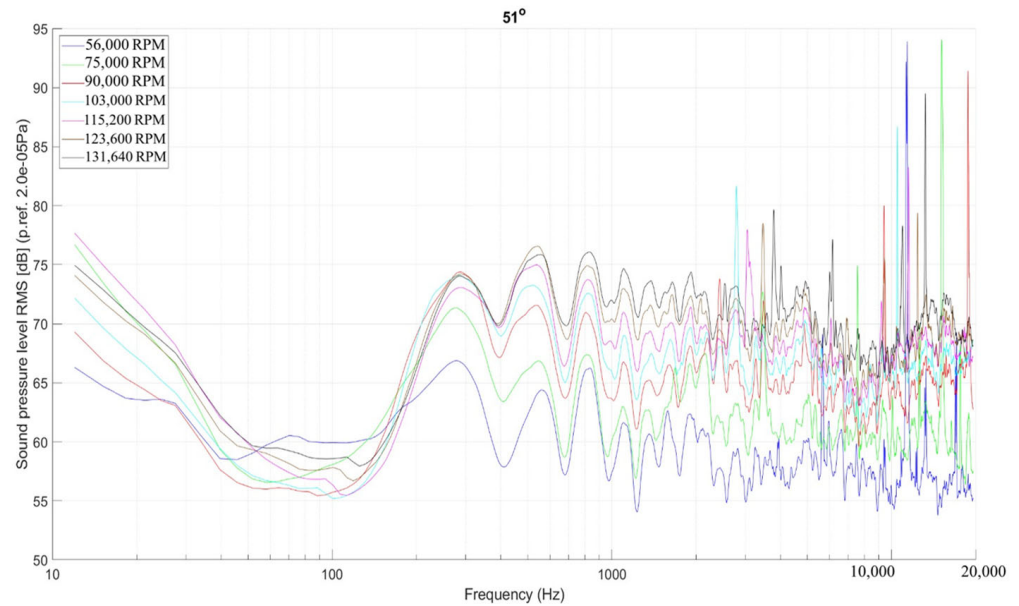


Figure 7. Comparative noise spectral analysis for the M3 microphone (51°) as a function of speed.

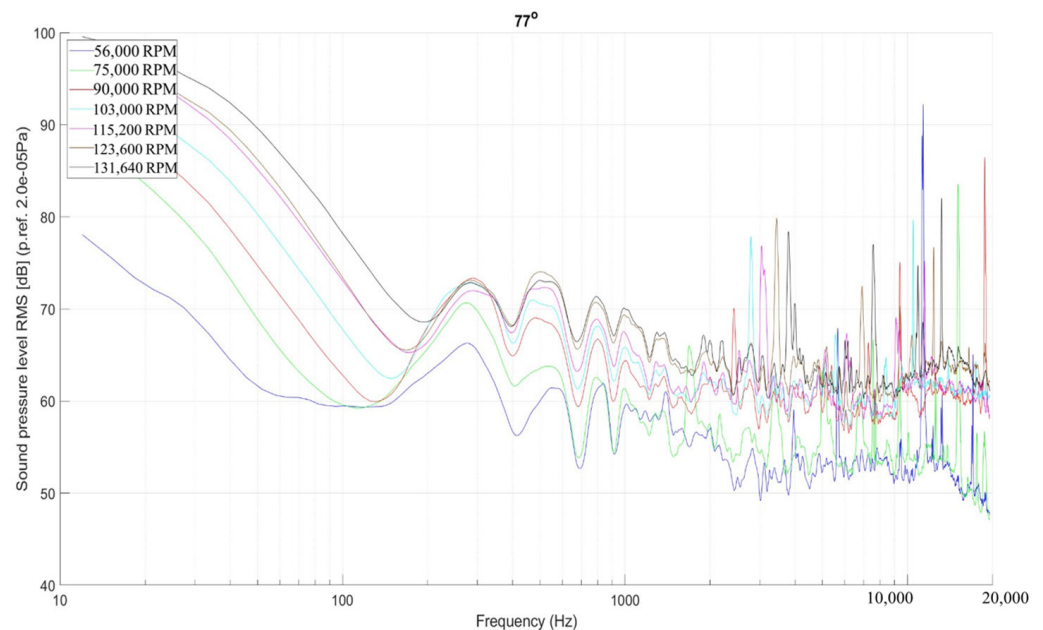


Figure 8. Comparative noise spectral analysis for the M4 microphone (77°) as a function of speed.

To get a comprehensive idea, the overall noise values (in the frequency domain from 16 to 20,000 Hz) for each RPM were averaged, resulting in the curved (purple) curve. It can be seen that the noise has the lowest value at a speed of 103,000 RPM.

The spectral analysis presented in Figures 5–12 explains the distinct character of the noise measured with microphones from 0° to 77° . Up to 103,000 RPM, the overall noise values from microphones from 0° to 77° are produced by the high-frequency components generated by the compressor impellers, with noise propagating outside from the engine intake. As the engine speed increases, these high frequencies exceed the upper frequency domain of 20 kHz, causing the overall noise level to drop to 103,000 RPM. On the back side of the test band, the noise has a linear increase from the idle regime to the maximum with no particularity.

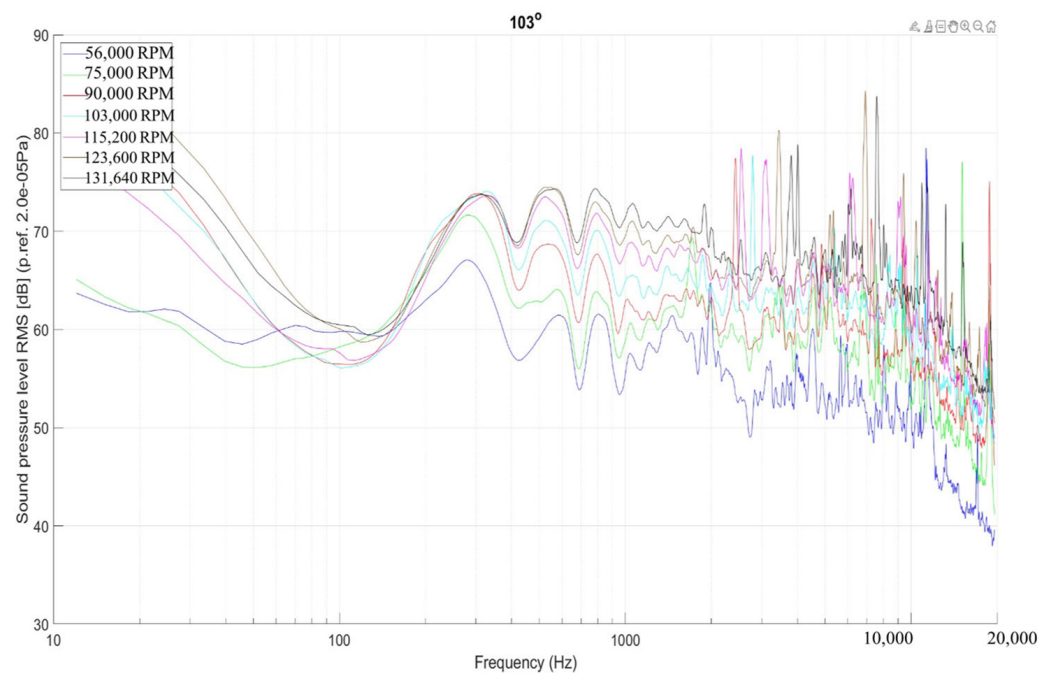


Figure 9. Comparative noise spectral analysis for the M5 microphone (103°) as a function of speed.

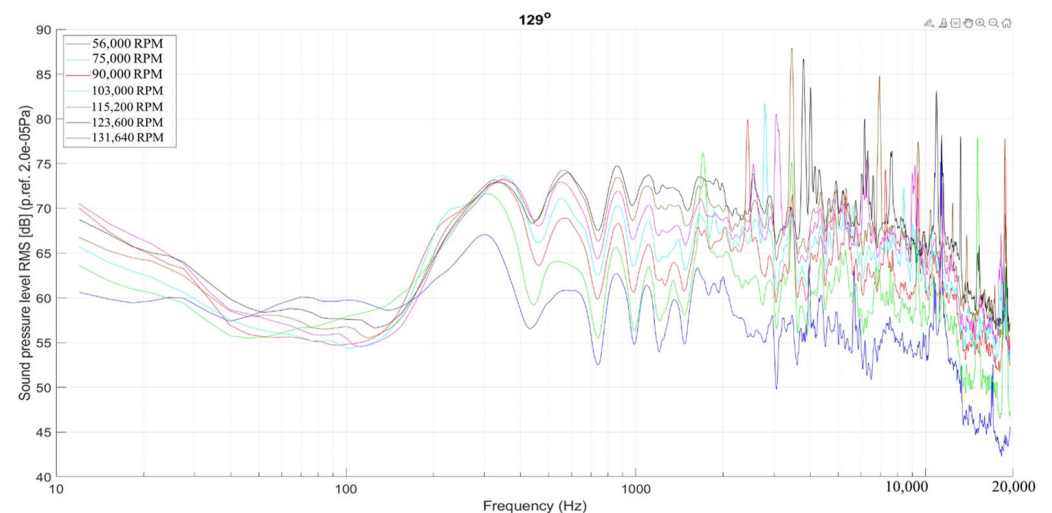


Figure 10. Comparative noise spectral analysis for the M6 microphone (129°) as a function of speed.

Based on the acoustic signals recorded close to the intake and exhaust, a detailed analysis of the main spectral components generated by the engine is further presented.

The second part of the study measures the sound pressure levels at the intake and exhaust of the turboshaft engine. This is crucial because observations indicate that the noise level produced by the entire assembly is quite high. Therefore, technical solutions are being sought to reduce the noise. Table 2 presents the global noise values measured at the positions of the microphones mounted near the intake and exhaust devices.

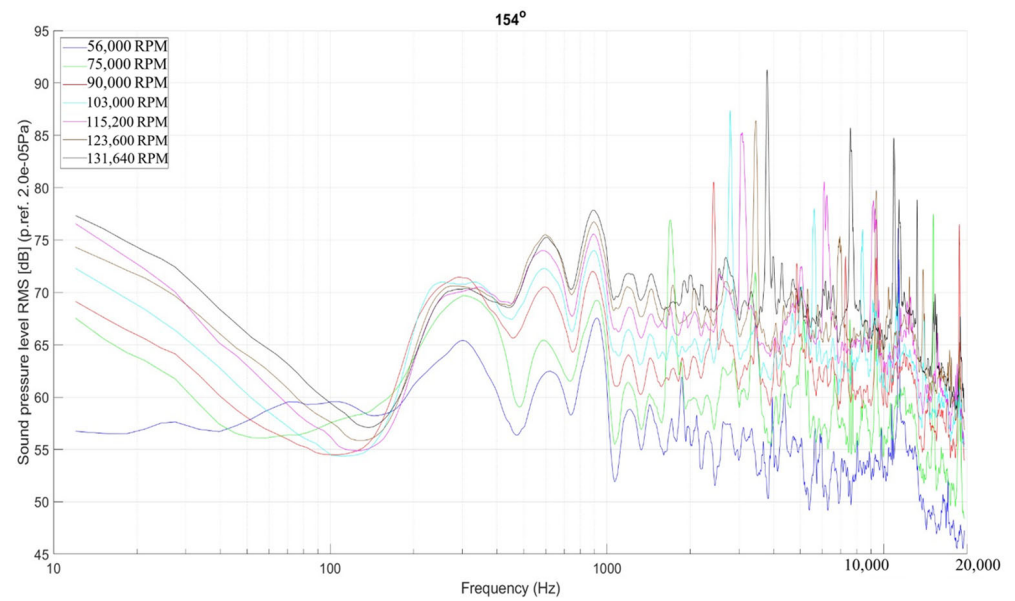


Figure 11. Comparative noise spectral analysis for the M7 microphone (154°) as a function of speed.

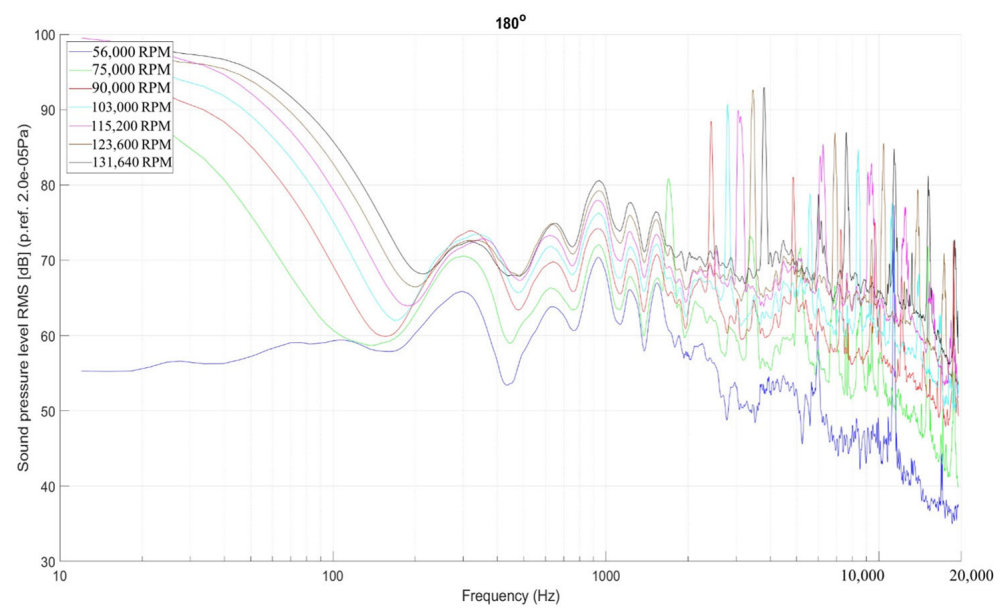


Figure 12. Comparative noise spectral analysis for the M8 microphone (180°) as a function of speed.

Table 2. Global noise values at a distance of 300 mm from the intake/exhaust.

| Speed [RPM] | OASPL [dB] | |
|-------------|------------|---------|
| | Intake | Exhaust |
| 56,000 | 123 | 101 |
| 75,000 | 125 | 104 |
| 90,000 | 130 | 108 |
| 103,000 | 116 | 110 |
| 115,200 | 118 | 111 |
| 123,600 | 119 | 113 |
| 131,640 | 120 | 114 |

The noise variation curves as a function of speed for both measurement points have been graphically represented; the results are shown in Figure 13.

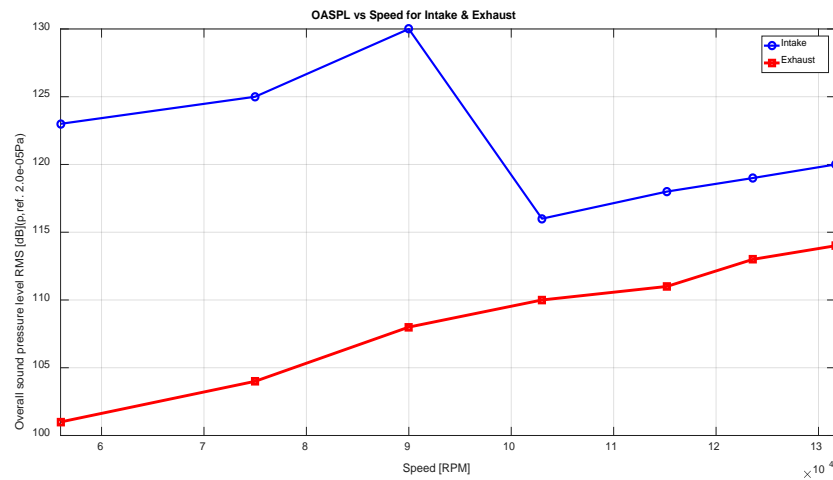


Figure 13. Variation in the global noise level near the intake and exhaust zone, depending on the speed of the microengine.

Regarding the exhaust noise, which is directly related to the speed [RPM], increasing the speed [RPM] leads to an approximately uniform increase in noise; from 101 dB at idle to 114 dB (that is, a 13 dB increase) at 131,640 RPM.

At the intake level, the noise is strongly influenced by the operating regime of the microengine; up to the regime of 90,000 RPM, the noise increases constantly (with a maximum value of 130 dB). This phenomenon occurs due to gas-dynamic phenomena and the operating regime of the compressor and turbine at these speeds, which generate noise at frequencies outside the recording spectrum of the microphones. After this point, the noise registers a sudden decrease (−15 dB) at the speed of 103,000 RPM, and finally, the noise increases linearly up to the maximum speed (120 dB). To better highlight the noise sources and the cause of the large differences in noise at low versus high regimes, spectral analyses of the acoustic signals near the intake device (Figure 14) and the signals from the exhaust area (Figure 15) are presented below.

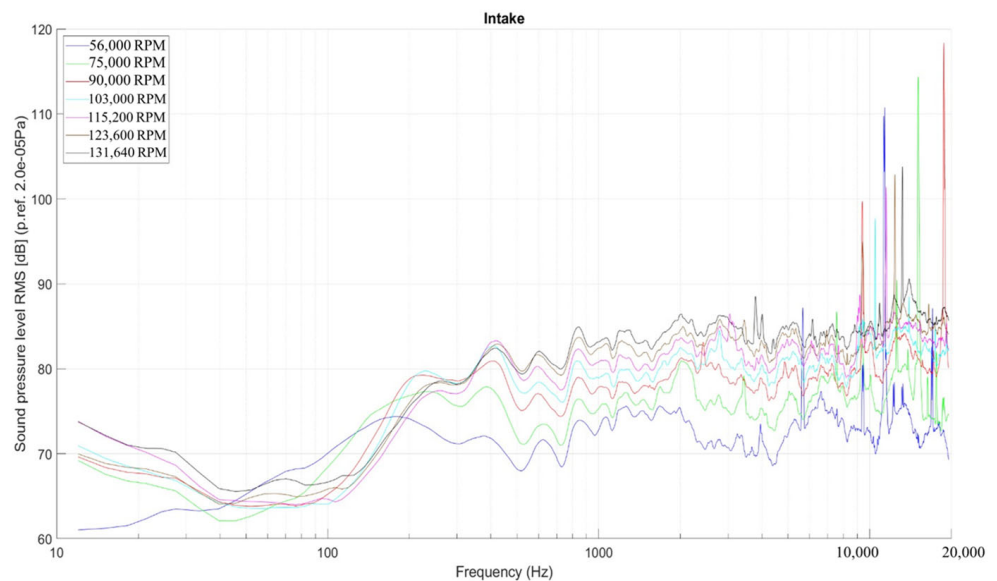


Figure 14. Comparative spectral analysis of the noise at 30 cm to the intake, depending on the speed.

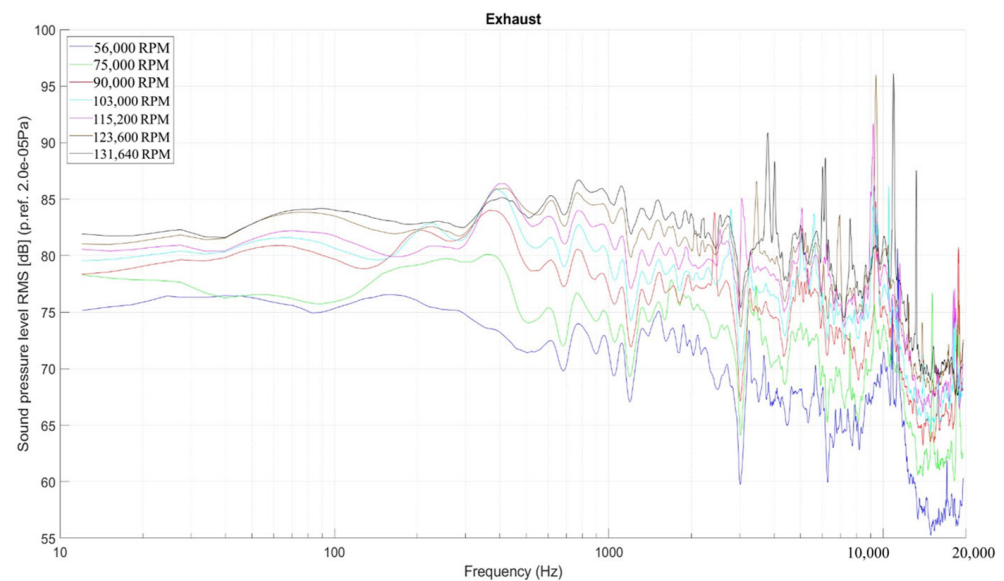


Figure 15. Comparative spectral analysis of noise at 30 cm from the EXHAUST, depending on the speed.

The following aspects of the noise can be observed: The spectral components corresponding to the speed have reduced amplitudes but are visible by performing an FFT zoom; analyzing the acoustic spectra and excluding the peaks, it is found that the noise increases with increasing speed, indicating a direct relationship between noise and speed; global values are strongly influenced by those tonal spectral components.

The interpretation of the spectral components with large amplitudes is as follows: For the speed of 56,000 RPM, the rotational speed component corresponds to a frequency of 933 Hz; from the spectrum, at the frequency of 5600 Hz, a BPF component can be observed, which corresponds to the number of compressor blades (6 blades); at the frequency of approximately 11,200 Hz (varying due to the inability of the automatic system to maintain a constant speed), there is a $2 \times$ BPF component. In the case of the speed of 75,000 RPM, the same BPF and $2 \times$ BPF components are observed, this time at higher frequencies, approximately 7560 Hz and 15,120 Hz, respectively; at the speed of 90,000 RPM, the BPF and $2 \times$ BPF components are at frequencies of approximately 9400 Hz and 18,800 Hz, respectively. For the other speeds, these components do not disappear, but due to the high speed, they move into the ultrasound domain, which is why the global noise values show significant decreases.

Figure 15 presents the spectral analysis of the noise at the exhaust level. In this area, the previously identified spectral components either have low amplitudes or are not visible, which supports the idea that those tonal components originate from the intake area.

Furthermore, in Figure 16, graphs are created for each speed, presenting the spectrum at the intake level compared to the acoustic spectrum at the exhaust level, thus highlighting the influence of intake noise on exhaust noise.

From Figure 16, it is primarily observed that the noise produced at the exhaust level contains low-frequency components (0–2000 Hz). The tonal components mainly originate from gas dynamic phenomena occurring in the compressor, with the noise propagating either directly to the exhaust or through the interior of the microengine, exiting through the exhaust. The spectral components of the turbine were not identified.

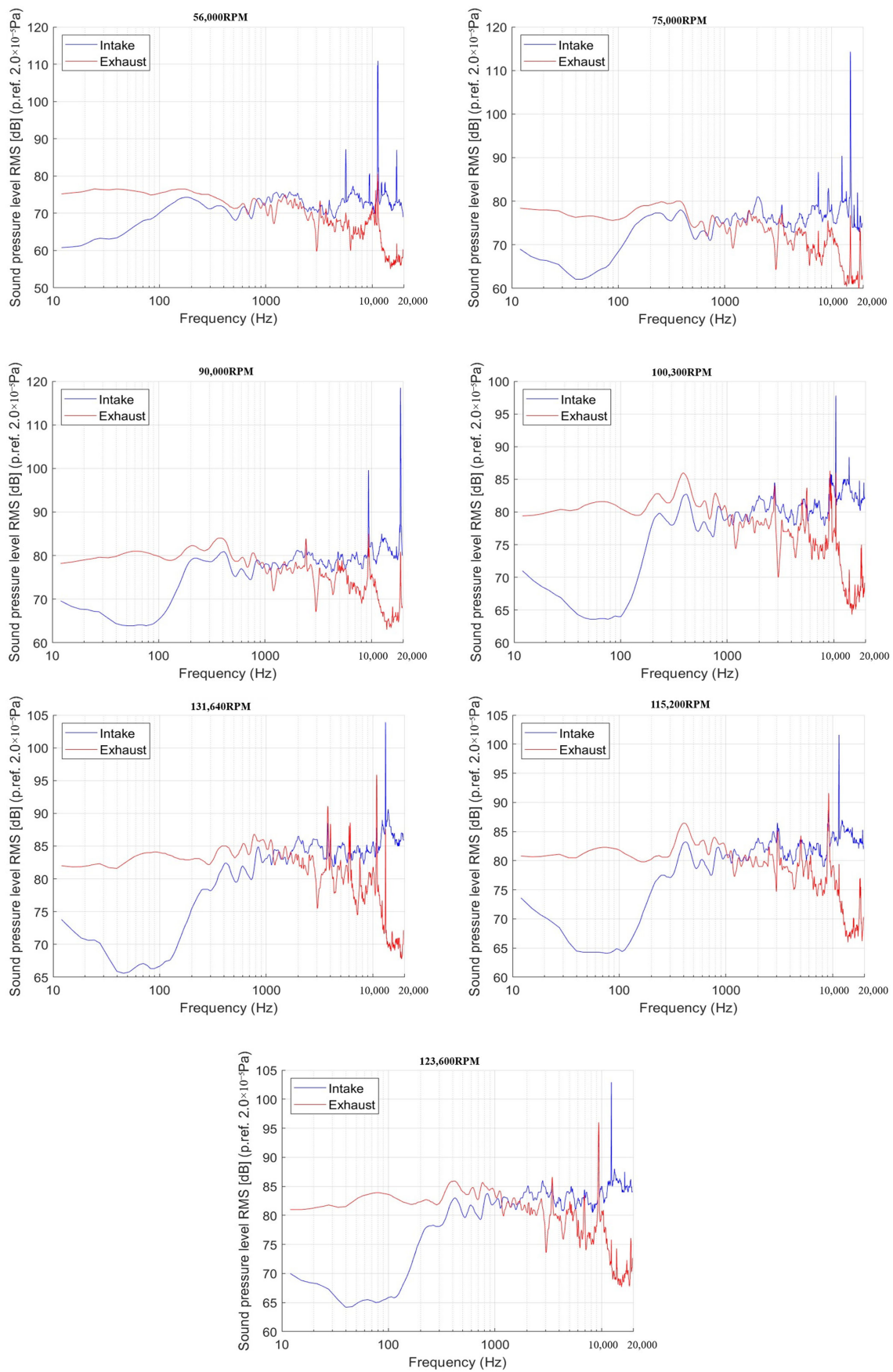


Figure 16. Spectral analysis of intake and exhaust noise for all tested speeds.

4. Conclusions

In this article, we made an acoustic analysis of a hybrid propulsion system developed to be implemented on a drone, which consists of a micro turboshaft coupled with a gearbox connected to an electric generator. The tests were performed in free-field conditions, far from other buildings, and on grassy land to avoid the influence of reflections and reverberation. For signal acquisition, an array of microphones was placed polar around the stand.

Regarding the current stand configuration, the analysis of the directivity curves does not provide significant information regarding the noise generated by the engine micro-engine. The noise generated by the whole set of acoustic sources has no prominent acoustic lobes, and up to 103,000 RPM, the noise levels have higher amplitudes in the front (intake region), reaching 113 dB, while in the back side (toward the fan), the noise reaches 97 dB. After this speed, the noise linear increases by 4 dB, from 103 dB at 103,000 RPM to 107 dB at 131,640 RPM.

Based on the spectral analyses performed for both the far-field acoustic signals (microphone polar array) and the near-field signals (microphones located near the intake and exhaust), it was found that the main sources with significant contributions to the overall noise come from the microengine compressor (gasodynamic phenomena in the fan -BPF and $2 \times$ BPF).

Thus, it was found that at the intake level, the main contribution to noise comes from the compressor's high-frequency components. In contrast, at the exhaust level, the noise primarily originates from the combustion chamber, which has low-frequency components (up to 2 kHz).

The results obtained in this study indicate that the noise level of a hybrid propulsion system for a drone is high, and solutions for noise reduction are required. Therefore, in future studies, noise attenuators will be designed for the intake and exhaust of the microturboengine-engine. Thus, reactive acoustic structures such as acoustic liners designed for high frequencies can be implemented for the intake, while other structures designed for low frequencies must be developed for the exhaust. These reactive structures must be designed to minimize weight as much as possible.

Another research direction is the compacting of the system and its implementation on a drone, a study that, among other things, will involve the acoustic analysis of the drone in various situations.

Author Contributions: Conceptualization, G.C., M.D. (Madalin Dombrovski) and G.-P.B.; methodology, T.F.F.; software, M.D. (Marius Deaconu), L.C. and A.-G.T.; writing—original draft preparation, G.C., M.D. (Marius Deaconu) and L.C.; writing—review and editing, G.C., M.D. (Madalin Dombrovski). All authors have read and agreed to the published version of the manuscript.

Funding: This work was carried out under the Nucleu Program of the National Research, Development, and Innovation Plan 2022–2027, supported by the Ministry of Research, Innovation, and Digitization (MCID), project no. PN23.12.03.01.

Data Availability Statement: The original contributions presented in the study are included in the article, further inquiries can be directed to the corresponding author/s.

Acknowledgments: The data presented and analyzed in this report were obtained with the help of INCDT COMOTI's Research and Experiments Center in the field of Acoustic and Vibrations staff and facility, and the work was carried out through the measurement equipment.

Conflicts of Interest: The authors declare no conflicts of interest.

References

1. Aasen, H.; Honkavaara, E.; Lucieer, A.; Zarco-Tejada, P.J. Quantitative remote sensing at ultra-high resolution with UAV spectroscopy: A review of sensor technology, measurement procedures, and data correction workflows. *Remote Sens.* **2018**, *10*, 1091. [[CrossRef](#)]
2. Abdullah, M.; Faizan, M.; Bhatti, M.Y.; Hasham, H.J. System design and analysis of hand lunched UAV. In Proceedings of the 14th International Bhurban Conference on Applied Sciences and Technology (IBCAST), Islamabad, Pakistan, 10–14 January 2017; pp. 551–560.

3. Badea, G.P.; Frigioescu, T.F.; Dombrovski, M.; Cican, G.; Dima, M.; Anghel, V.; Crunteanu, D.E. Innovative Hybrid UAV Design, Development, and Manufacture for Forest Preservation and Acoustic Surveillance. *Inventions* **2024**, *9*, 39. [[CrossRef](#)]
4. Zhang, B.; Song, Z.; Zhao, F.; Liu, C. Overview of Propulsion Systems for Unmanned Aerial Vehicles. *Energies* **2022**, *15*, 455. [[CrossRef](#)]
5. Frigioescu, T.; Dombrovski, M.; Badea, G.; Cican, G.; Condruz, R.; Crunteanu, D.-E. Development of an Uav platform for autopilot implementation and validation. *TURBO* **2023**, *X*, 2.
6. Boukoberine, M.N.; Zhou, Z.; Benbouzid, M.A. Critical review on unmanned aerial vehicles power supply and energy management: Solutions, strategies, and prospects. *Appl. Energy* **2019**, *255*, 113823. [[CrossRef](#)]
7. Kong, X.; Zhang, Z.; Lu, J.; Li, J.; Yu, L. Review of electric power system of distributed electric propulsion aircraft. *Acta Aeronaut. Astronaut. Sin.* **2018**, *39*, 021651.
8. Kong, X.; Liu, H. Research progress of key technologies of aviation piston engine for UAV. *Small Intern. Combust. Engine Veh. Tech.* **2021**, *50*, 3.
9. Mikalsen, R.; Roskilly, A.P. A review of free-piston engine history and applications. *Appl. Therm. Eng.* **2007**, *27*, 2339–2352. [[CrossRef](#)]
10. Frigioescu, T.-F.; Badea, G.P.; Dombrovski, M.; Condruz, M.R.; Crunteanu, D.-E.; Cican, G. The Design and Development of a UAV's Micro-Turbogenerator System and the Associated Control Testing Bench. *Electronics* **2023**, *12*, 4904. [[CrossRef](#)]
11. Telli, K.; Kraa, O.; Himeur, Y.; Ouamane, A.; Boumehraz, M.; Atalla, S.; Mansoor, W. A Comprehensive Review of Recent Research Trends on Unmanned Aerial Vehicles (UAVs). *Systems* **2023**, *11*, 400. [[CrossRef](#)]
12. Chen, P.; Pai, P.; Yang, C.; Huang, K. Development of transmission systems for parallel hybrid electric vehicles. *Appl. Sci.* **2019**, *9*, 1538. [[CrossRef](#)]
13. Lieh, J.; Spahr, E.; Behbahani, A.; Hoying, J. Design of hybrid propulsion systems for unmanned aerial vehicles. In Proceedings of the 47th AIAA/ASME/SAE/ASEE Joint Propulsion Conference & Exhibit, San Diego, CA, USA, 31 July–3 August 2011; p. 6146.
14. Schäffer, B.; Pieren, R.; Heutschi, K.; Wunderli, J.M.; Becker, S. Drone Noise Emission Characteristics and Noise Effects on Humans—A Systematic Review. *Int. J. Environ. Res. Public Health* **2021**, *18*, 5940. [[CrossRef](#)]
15. Sun, J.; Yonezawa, K.; Shima, E.; Liu, H. Integrated Evaluation of the Aeroacoustics and Psychoacoustics of a Single Propeller. *Int. J. Environ. Res. Public Health* **2023**, *20*, 1955. [[CrossRef](#)]
16. Tejera-Berengue, D.; Zhu-Zhou, F.; Utrilla-Manso, M.; Gil-Pita, R.; Rosa-Zurera, M. Analysis of Distance and Environmental Impact on UAV Acoustic Detection. *Electronics* **2024**, *13*, 643. [[CrossRef](#)]
17. Yamada, T.; Itoyama, K.; Nishida, K.; Nakadai, K. Assessment of Sound Source Tracking Using Multiple Drones Equipped with Multiple Microphone Arrays. *Int. J. Environ. Res. Public Health* **2021**, *18*, 9039. [[CrossRef](#)] [[PubMed](#)]
18. Read, D.R.; Senzing, D.A.; Cutler, C.; Elmore, E.; He, H. *Noise Measurement Report: Unconventional Aircraft—Choctaw Nation of Oklahoma: July 2019*; DOT/FAA/AEE/2020-04; U.S. Department of Transportation, John A. Volpe National Transportation Systems Center: Cambridge, MA, USA, 2020.
19. EUROCONTROL. Aircraft Noise and Performance (ANP) Database. Available online: <https://www.easa.europa.eu/en/domains/environment/policy-support-and-research/aircraft-noise-and-performance-anp-data/anp-legacy-data> (accessed on 22 May 2024).
20. Civil Aviation Authority. *Departure Noise Mitigation: Main Report*; Civil Aviation Authority: West Sussex, UK, 2018.
21. Gwak, D.Y.; Han, D.; Lee, S. Sound quality factors influencing annoyance from hovering UAV. *J. Sound Vib.* **2020**, *489*, 115651. [[CrossRef](#)]
22. Torija, A.J.S.; Rod, H.; Lawrence, J.L. Psychoacoustic Characterisation of a Small Fixed-Pitch Quadcopter. In Proceedings of the INTER-NOISE and NOISE-CON Congress and Conference Proceedings, InterNoise19, Madrid, Spain, 16–19 June 2019; Institute of Noise Control Engineering: Madrid, Spain, 2019; pp. 1884–1894.
23. Alexander, W.N.; Whelchel, J. Flyover Noise of Multi-Rotor sUAS. In Proceedings of the INTER-NOISE and NOISE-CON Congress and Conference Proceedings, Madrid, Spain, 16–19 June 2019; Volume 259, pp. 2548–2558.
24. Cabell, R.; McSwain, R.G.; Grosveld, F. Measured Noise from Small Unmanned Aerial Vehicles. In Proceedings of the NOISE-CON 2016, Providence, RI, USA, 13–15 June 2016.

Disclaimer/Publisher's Note: The statements, opinions and data contained in all publications are solely those of the individual author(s) and contributor(s) and not of MDPI and/or the editor(s). MDPI and/or the editor(s) disclaim responsibility for any injury to people or property resulting from any ideas, methods, instructions or products referred to in the content.